Bulgarian Chemical Communications, Volume 50, Special Issue F (pp. 211–218) 2018

Preparation and antimicrobial properties of silver nanoparticles supported by natural zeolite clinoptilolite

M. I. Panayotova[1*], N. N. Mintcheva[1], O. T. Gemishev[2], G. T. Tyuliev[3], G. D. Gicheva[1], L. P. Djerahov[1]

[1] *Department of Chemistry, University of Mining and Geology, Sofia 1700, Bulgaria*
[2] *Faculty of Biology, Sofia University ''St. Kl. Ohridski'', Sofia 1000, Bulgaria*
[3] *Institute of Catalysis, Bulgarian academy of sciences, Sofia 1113, Bulgaria*

Received October 15, 2018; Accepted December 15, 2018

Nanocomposites (AgNPs-zeolite) comprising of silver nanoparticles supported by the natural Bulgarian zeolite clinoptilolite have been prepared by two-step synthesis: silver ions (Ag^+) immobilization on the zeolite followed by their thermal reduction and formation of silver nanoparticles (AgNPs). The structure and surface chemistry of as-prepared nanocomposites, morphology and size distribution of the obtained AgNPs were characterized by various methods (XRD, BET, XPS, SEM, and TEM). SEM and EDS analyses have shown around 11 wt% Ag which is uniformly dispersed in the zeolite host. On TEM images it can be seen that the composites contain small (3–5 nm) AgNPs situated in the microstructural defects of the zeolite crystals, and bigger AgNPs (20–25 nm) that are located on the surface of zeolite crystallites. The AgNPs-zeolite composites, at low amount added to Peptone water, cease the *Escherichia coli* cell growth. The synthesized AgNPs-clinoptilolite composites could find an application in the water disinfection.

Keywords: silver nanoparticles, nanocomposites, AgNPs-zeolite, antimicrobial activity.

INTRODUCTION

The antimicrobial action of silver species is well known. In doses used, silver is a non-toxic to human, which makes it desirable for applications in sensitive media such as drinking water, foods, etc. It is reported that the high specific surface area of silver nanoparticles (AgNPs) leads to higher bactericide activity in comparison with bulk silver metal [1]. In order to be applied effectively for water disinfection, nanoparticles must be protected from aggregation and supported on substrates such as polymers [2], clays [3, 4] or their mixtures [5]. Zeolites are aluminosilicate mesoporous ion exchange materials that have been used to host a variety of metallic species, including silver. Due to their stable network of hollow channels and pores and their thermal stability, natural and synthetic zeolites are ideal templates for formation and growth of various nanoparticles. In addition, small nanoparticles are physically prevented from aggregation to larger nanoparticles or micron-sized particles [6]. Thus, the zeolites have attracted the attention as promising material for producing composite materials bearing AgNPs.

Composites containing AgNPs and different synthesized zeolites (A, L, ZSM-5, and Y), have been prepared in order to test their antibacterial properties [6–10]. The number of works, where natural zeolites are used, is relatively low [11–14]. It is worth to mention that synthetic zeolites are manufactured by energy consuming processes, using chemicals, and usually these materials have silica to alumina ratio of 1 to 1, while in natural clinoptilolite type zeolites this ratio is around 5 to 1. That's why natural clinoptilolite and its composites are more acid resistant and do not break down in a mild acidic media, where synthetic zeolites do. Natural clinoptilolite is nontoxic and it is widely used as a soil amendment and as a food additive. Moreover, zeolites with low field strength and with higher Si content, such as clinoptilolite, are more selective towards cations with lower charge density, such as Ag^+ [15].

All above-described advantages render clinoptilolite a valuable material for preparing AgNPs-clinoptilolite composites and have attracted our attention. Herein we present the preparation of AgNPs-zeolite nanocomposites by thermal reduction of Ag-loaded zeolite. TEM images and XPS

* To whom all correspondence should be sent:
E-mail: marichim@mgu.bg

spectra confirm the formation of ultra-small Ag nanoparticles. Ag-containing composites demonstrate rapid antimicrobial activity against *Escherichia coli*.

EXPERIMENTAL

Natural zeolitic rock from East Rhodopes region of Bulgaria was used. After milling, the fraction 0.09-0.325 mm was deployed. Zeolite was washed following procedure described in our previous work [16]. The zeolite chemical composition, determined by means of silicate analysis, is (in wt.%): SiO_2 – 70.19, Al_2O_3 – 10.90, CaO – 2.87, MgO – 0.51, K_2O – 3.41, Na_2O – 0.36, Fe_2O_3 – 0.28, MnO – 0.04, TiO – 0.06, P_2O_3 < 0.05, SO_3 < 0.05, LOI – 10.99. The theoretical cation exchange capacity (TCEC) was found to be 211 meq/100 g zeolite. It is in the same range as the TCEC determined by other authors for clinoptilolite from nearby geographic region [15, 17, 18]. The XRD analysis of washed material has revealed that it contains 73% zeolite clinoptilolite.

Zeolite was loaded with silver ions (Ag^+) by placing it in contact with 0.1 M and 0.01 M $AgNO_3$ solutions at solid to liquid ratio (m:v) = 1:20 for 4 hours. At the end of contact time, the $AgNO_3$ solution was analyzed by ICP-OES for Na^+, K^+ and Ca^{2+}. Ag-loaded zeolite was washed with distilled water till negative reaction for Ag^+ in washings was observed and then it was dried at 50 °C overnight. During all experiments precautions were taken due to silver light sensitivity. Higher loading of zeolite with Ag^+ has been achieved at higher initial concentration of $AgNO_3$ solution (e.g. 0.1 M). More detail description on the preparation of the Ag-loaded zeolite can be found in our previous work [16]. Samples of the Ag-loaded zeolite were heated at temperatures 200, 400 and 600 °C under air conditions for 2 hours. Thus obtained composites were denoted respectively as "z – initial Ag concentration – heating temperature". For example, z-0.1-200 means "Ag-loaded zeolite, obtained by contacting the zeolite with 0.1 M $AgNO_3$ solution and then heating the material at 200 °C for 2 hours".

The samples obtained were subjected to XRD (BRUKER D2 Phaser, Cu/Ni radiation, l=1.54184 Å, 30 kV, 10 mA, 2 theta – 5–70, time 1720 s) and SEM-EDS (JEOL – JSM-6010PLLIS/LA) analyses. The specific surface area of samples was measured by applying the Brunauer, Emmett and Teller (BET) method and using Quantachrome NOVA 1200e Analyzer working with N_2. The samples were preliminary heated at 200 °C, for 16 hours under vacuum. The XPS measurements were carried out in the analysis chamber of electron spectrometer Escalab-MkII (VG Scientific) with a base pressure of 1×10^{-10} mbar. The spectra were excited with AlK_α radiation (hν = 1486.6 eV) at instrumental resolution of 1.1 eV as measured by FWHM of $Ag3d_{5/2}$ photoelectron line. Energy calibration was made by using the strongest O1s line in the spectra centered at 532.7 eV. In order to minimize the effect of irradiation during data acquisition, a low power (5 mA/6 kV) for the X-ray source was used. TEM analysis was carried out on JEOL, model JEM 2100, 200 kV analytical electron microscope.

E. coli strain 3398 was pre-grown on a Luria agar for 16 h at 37 ± 0.1 °C to obtain cultures in a log phase of growth. Antibacterial activity was investigated in peptone water (PW) that was prepared by dissolving the 10.0 g of peptone (Sigma Aldrich) and 0.5 g of NaCl (p.a.) in 1 L distilled water (pH = 7.0). PW and tested materials were sterilized by autoclaving at 121 °C, 20 min. In each one of fifteen sterile tubes 10 mL of PW were poured. First three tubes with PW and without *E. coli* were used as negative control. Tested AgNPs – clinoptilolite composites were added in concentration 0.1 wt% to the other three sets each one of three tubes, respectively z-0-400, z-0.1-400 and z-0.1-600. 10 mL of *E. coli* cell suspension, prepared in PW and containing 10^5 colony forming units per milliliter were added to all tubes, except the first three (i.e. the negative control). The tubes containing only PW and *E. coli* suspension but without any addition of zeolite represented a positive control. All tubes were placed in a thermostat at temperature 37 °C. Samples were taken at 0, 1, 3, 6, 12 and 24 hours. To monitor the cell growth, the samples' optical density (OD) was measured at 630 nm. The data from the three parallel samples are reported after averaging them.

RESULTS AND DISCUSSION

X-ray diffraction

XRD patterns of unloaded zeolite and Ag-loaded-zeolites annealed at 400 °C for 2 h are presented in Fig. 1.

The peak positions of pure zeolite and silver loaded zeolite are essentially identical which indicates that the zeolite structure was preserved after silver immobilization**.** This shows that the zeolite material can be used as an effective support for the fabrication of AgNPs-zeolite composites. However, the intensity of the characteristic clinoptilolite peaks decreases slightly with increasing the silver content in the composite. Since the clinoptilolite is structurally stable up to 750 °C [15] this effect may be due to some changes of charge distribution and electrostatic fields occurring when exchangeable zeolite ions are replaced by silver ions, as stated also by

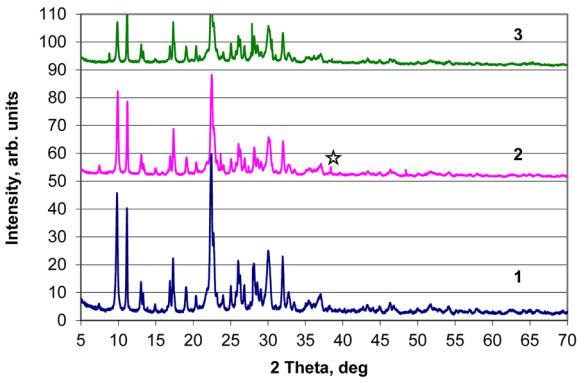

Fig. 1. X-ray diffraction patterns of unloaded and Ag-loaded samples: *1* – z-0-400; *2* – z-0.01-400; *3* – z-0.1-400.

other authors [9]. Characteristic silver peaks are not observed for the sample z-0.01-400 (zeolite bearing lower amount of silver), and the Ag peak with the maximum intensity at 2Θ = 38.4° is barely recognizable for z-0.1-400 sample. Other characteristic peaks of Ag (according to JCPDS card No.04-0783) are not observed, probably due to the relatively low amount of silver in the zeolite. Similar effects were observed also by other authors [6, 12, 19].

For further characterization of AgNPs-zeolite composites we chose the ones with higher Ag-loading, namely samples z-0.1-200; z-0.1-400 and z-0.1-600 (treated at temperatures 200, 400 and 600 °C).

BET surface

Data on the BET surface of pure and Ag^+-loaded zeolite, heated at temperatures 200, 400, 600 °C, i. e. in the range of the clinoptilolite thermal stability, are presented in Table 1.

The values of the BET surface determined for the pure zeolite are in the range of BET values obtained by other authors for clinoptilolite from the nearby geographic region (19.6 m^2/g – [20] and 30 m^2/g – [21]). The relatively low values found for specific surface area are due to the fact that N_2 cannot enter into voids with diameter less that 2 nm [21], such as channels of the natural clinoptilolite and it is adsorbed mainly on the external surface of the zeolite crystals [22].

Samples heating lead to decrease in the BET surface with increase of temperature in similar manner for the non-loaded and silver-loaded zeolite. BET analysis showed a reduction in surface area of the silver bearing zeolite with approximately 20% compared to non-treated zeolite, most probably because the formed AgNPs could cover some of the zeolite sites. This could be explained by the exchange of K^+ and Na^+ ions by Ag^+ ions and further reduction of Ag^+ to Ag^o. K^+ has ionic radius of 152 pm, the ionic radius of Na^+ is 116 pm, whereas Ag^o has an atomic radius of 165 pm [23, 24]. Moreover, formation of silver clusters and growth of AgNPs partially blocks the zeolite pores, thus the specific surface area decreases and the measured pores volume is smaller too. The exchange of K^+ for Ag^+ has been confirmed by the ICP analysis.

XPS analyses

XPS spectra (Ag3d photoelectron and AgMNN Auger-lines) of studied composites, prepared by silver-loaded zeolite annealing at different temperatures, are presented in Fig. 2. The sample z-0.1-600 was additionally crushed in agate mortar before insertion into the analysis chamber for analysis. Results are presented in Fig. 3 and Table 2.

As shown in Fig. 2, the XPS spectra of Ag3d region exhibit a peak at binding energy (BE) of 369.3 eV. It could be assigned to Ag^o, thus indicating that silver presents as Ag^o on the zeolite surface. The binding energy of the Ag3d5/2 and Ag3d3/2 doublet for metalic silver is observed at 368.3 eV and 374.3 eV, respectively [25, 26]. Shift to higher BE could be due to the fact that silver is in the form of small particles, only few nanometers in size. In Ag3d region two main peaks centered at 368.7–368.8 eV for Ag3d5/2 and 374.7–374.8 eV for Ag3d3/2 have been reported for AgNPs-faujasite zeolite compos-

Table 1. BET surface of the studied samples and pores volume

Zeolite type	z-0-xxx		z-0.1-xxx	
Temperature, °C	S_{BET}, m^2/g	V_p, cm^3/g	S_{BET}, m^2/g	V_p, cm^3/g
200	22	0.09	18	0.07
400	20	0.08	16	0.07
600	18	0.08	14	0.06

xxx – the corresponding temperature.

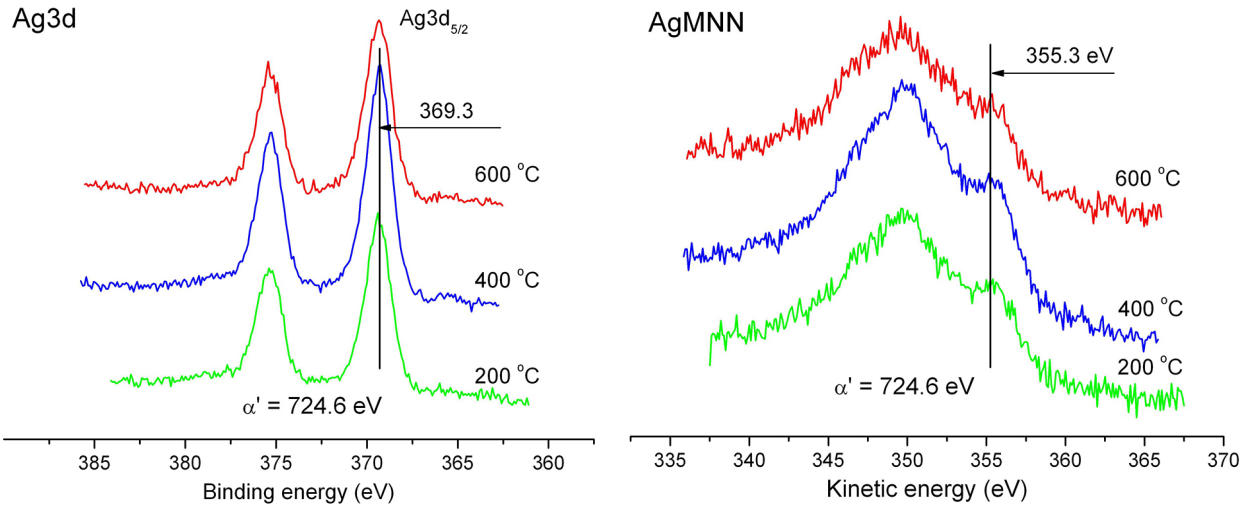

Fig. 2. XPS spectra of composites z-0.1-200, z-0.1-400, z-0.1-600 – Ag3d photoelectron and AgMNN Auger spectra.

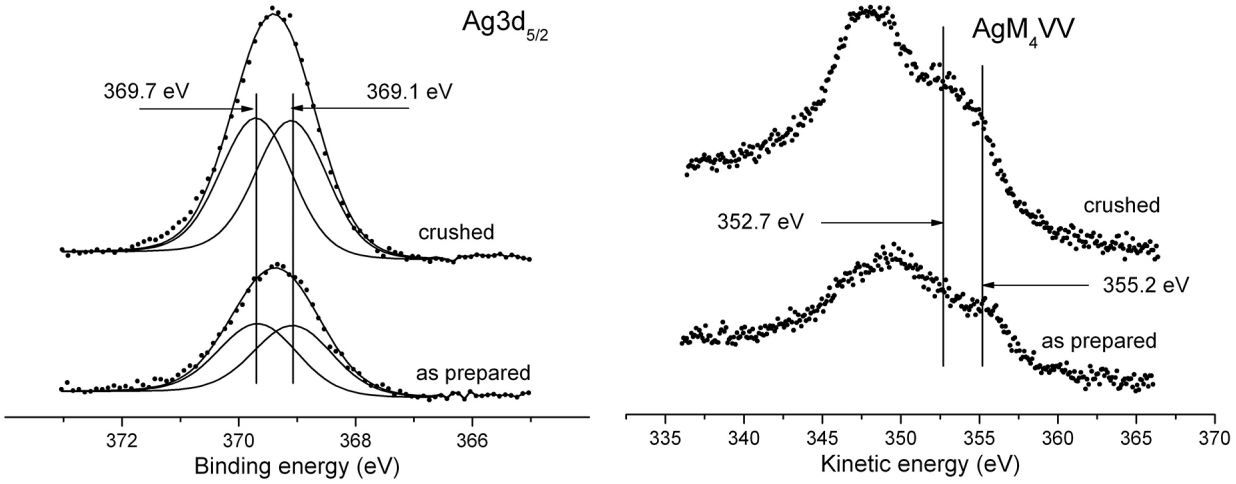

Fig. 3. XPS spectra of composite z-0.1-600 – Ag3d photoelectron and AgMNN Auger spectra of as prepared and crushed sample.

Table 2. Surface composition (in atomic %) for z-0.1-600 sample in as prepared form and after crushing in agate mortar before insertion into the analysis chamber for analysis

Sample	O	Si	Al	Fe	Mg	K	Ca	Cl	Ag
As prepared	58.5	30	5.43	0.81	1.3	0.7	0.2	0.2	2.84
Crushed	56.1	29.7	5.08	0.5	0.93	1	0.52	0.95	5.17

ite [12] for particles bigger than the described in the present paper. Practically, the temperature at which the silver-loaded zeolite is annealed does not impact the BE, as it can be seen in Fig. 2. According to the literature, the standard Auger parameter of metallic state silver is 726.0 eV, and that of silver ion is 724.0 eV [12]. The calculated Auger parameters for our sample is 724.6 eV thus suggesting that the silver is under different forms in the composite. Figure 3 further confirms that both metallic ($Ag3d_{5/2}$ at 369.1 eV (BE), and AgM_4VV at 355.2 eV (KE)) and ionic silver (369.7 eV and 352.7 eV respectively) present in the samples. The presence of Ag^o particles in the zeolite implies that a thermal reduction

process of Ag^+ has occurred under air conditions in the Ag^+-bearing zeolite. Similar processes under oxidative conditions were observed also by other authors [8, 11].

Data presented in Fig. 3 (peaks' intensity) and Table 2 show that the additional crushing leads to an increase of Ag3d peaks indicating higher abundance of AgNPs on the surface. This could be assigned to an additional exposure of silver nanoparticles which come from the zeolite cavities on the surface.

SEM and EDS analyses

Scanning electron micrographs of the studied samples (z-0-400 and z-0.1-400) are presented in Figs. 4 and 5 respectively. The morphology of zeolite is changed after its loading with silver, as it can be seen in Fig. 4. Treatment in $AgNO_3$ solution for 4 hours to achieve silver ions immobilization causes size decrease of the zeolite particles. EDS spectrum of AgNPs-clinoptilolite composite and the mapping with respect to Ag are presented in Fig. 6. Elemental composition of pure zeolite and AgNPs-clinoptilolite composite are compared in Table 3. EDS elemental mapping (Fig. 6b) shows that silver is uniformly dispersed in the zeolite host. EDS analysis indicated the presence of around 11 wt.% Ag on the surface of sample z-0.1-400.

TEM analyses

Transmission electron microscope images of the AgNPs-zeolite composite are presented in Fig. 7.

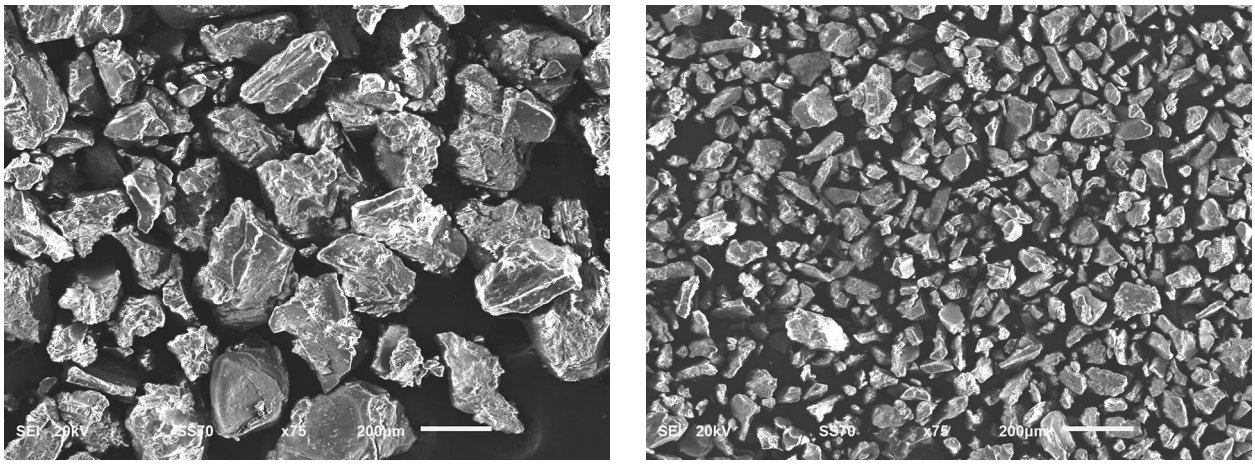

a) *b)*

Fig. 4. Scanning electron micrographs – overview of samples (*a*) z-0-400, (*b*) z-0.1-400.

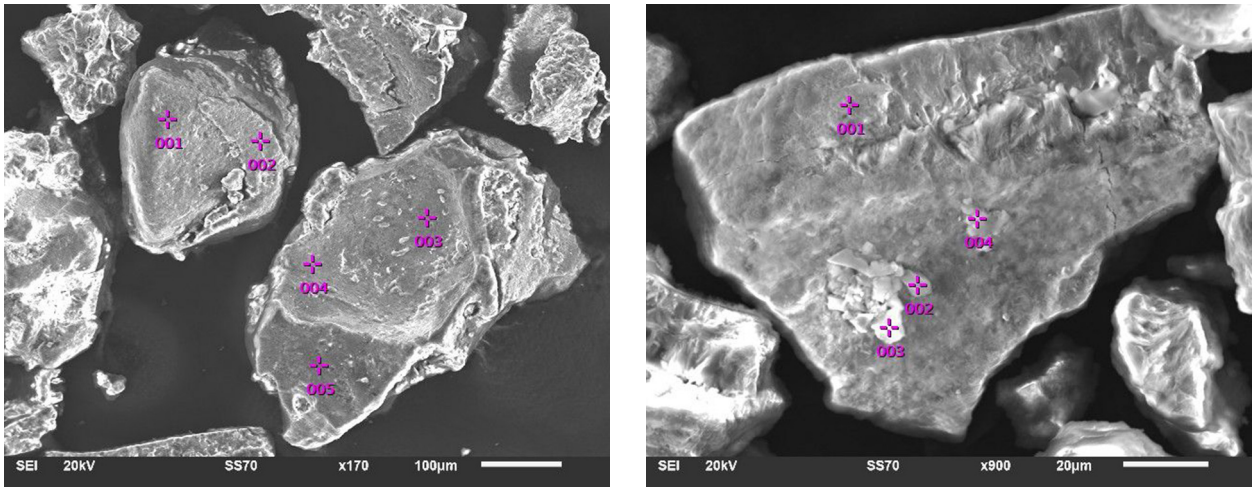

a) *b)*

Fig. 5. Scanning electron micrographs of samples (*a*) z-0-400, (*b*) z-0.1-400.

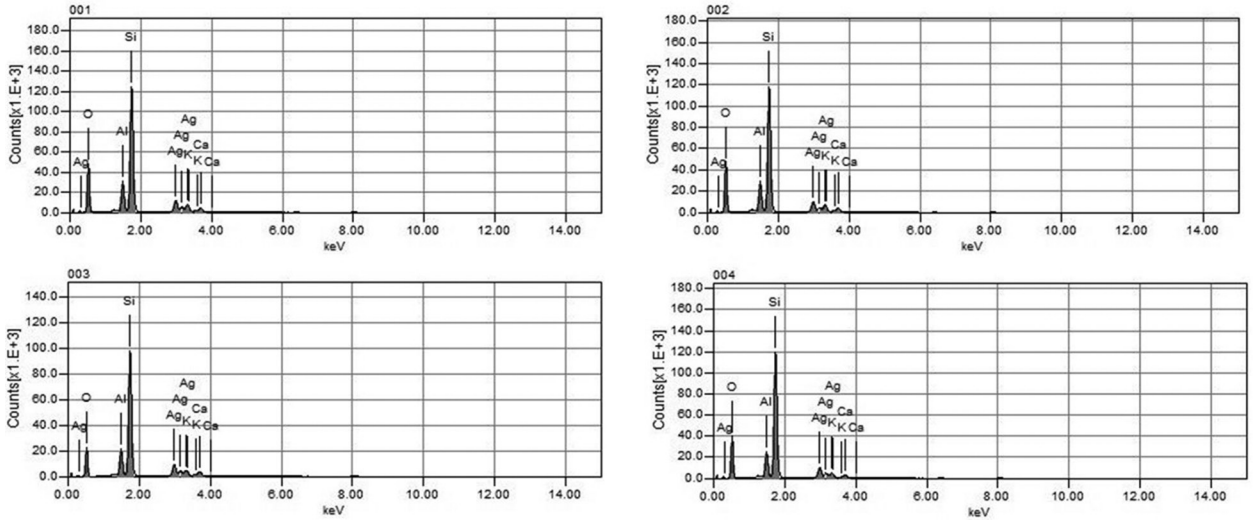

a)

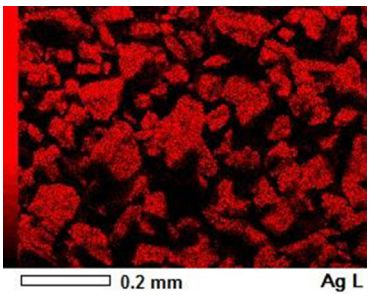

b)

Fig. 6. EDS and SEM results: (*a*) EDS spectrum of z-0.1-400 sample – points 1-4 on Fig. 4b, (*b*) Elemental mapping (Ag) of z-0.1-400 sample.

Table 3. Elemental composition (wt.%) of samples z-0-400, z-0.1-400 based on EDS data

Sample z-0-400						Sample z-0.1-400						
Point[1]	O	Si	Ca	Al	K	Point[2]	O	Si	Ca	Al	K	Ag
1	47.57	38.13	2.89	6.78	4.62	1	46.92	31.28	1.64	6.20	2.67	11.28
2	50.99	36.96	2.64	5.82	3.58	2	48.00	31.52	1.60	6.24	2.65	9.98
3	46.68	39.43	3.17	6.39	4.33	3	38.34	37.25	2.34	6.47	2.07	13.53
4	48.24	37.65	2.95	6.93	4.24	4	44.90	34.25	1.47	5.84	1.83	11.70
5	47.02	45.02	1.71	3.58	2.67	*Aver.*	44.54	33.58	1.76	6.19	2.31	11.62
Aver.	48.10	39.44	2.67	5.90	3.89							

[1] – see Fig. 5a; [2] – see Fig. 5b.

TEM analysis indicates that AgNPs could be observed both on the crystallites' surface (Fig. 7a) and on the zeolite crystals (Fig. 7b). AgNPs located on the crystallites are bigger (20–25 nm) than those situated on the active sites of the zeolite crystals (3–5 nm). The primary building units of zeolites are the SiO_4 and AlO_4 tetrahedra. They are connected via oxygen into secondary building units, which are then linked into a three-dimensional crystalline structure of zeolite. The building units are connected in a way forming three types of channels. Two of them are parallel, and made of ten and eight-membered rings of Si/AlO_4. The free diameters of the 10-ring channels are 0.44×0.72 nm, while the free diameters of the 8-member ring channels are 0.41×0.47 nm. The third type of channels is defined

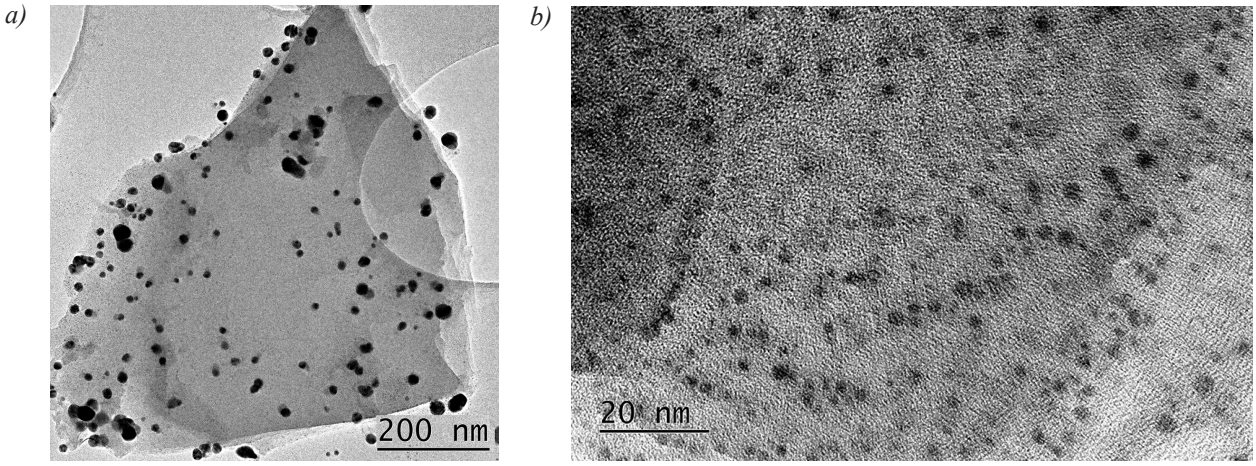

Fig. 7. Transmission electron microscope images of the AgNPs-zeolite composite material (sample z-0.1-400).

by eight-membered rings with free diameters 0.40 × 0.55 nm. These channels are vertical [15]. The described structure defines primary porosity (or microporosity) of zeolite mineral crystals, where the AgNPs cannot be aligned. Additionally, clinoptilolite possesses secondary structure of fracture-type porosity, with pores from 25–50 nm to 100 nm in size, shaped between clinoptilolite crystals [21], which are capable to accommodate AgNPs formed by thermal reduction of incorporated silver ions. Thus, considering the zeolite structure we believe that the small-sized AgNPs are located on the surface of zeolite crystals and are uniformly distributed, while the bigger AgNPs are formed in the mesoporous structure of zeolite crystallites by aggregation.

Antibacterial activity

Antibacterial activity of pure zeolite and two Ag-loaded zeolite samples (z-0.1-400 and z-0.1-600) against *E. coli* strain 3398 were tested. Data on the antibacterial activity of the AgNPs-zeolite composite material are presented in Fig. 8. As it can be seen in Fig. 8, the synthesized AgNPs-zeolite composite is an efficient bactericide material with respect to *E. coli* even in low concentration. There is no growth *E. Coli* for samples z-0.1-400 and z-0.1-600. The measured optical density of the samples coincides with that of the positive control at the zero hour. Destruction of *E. Coli* present in nutritive media by silver nanoparticles supported on Mexican clinoptilolite have been reported by other authors [13]. AgNPs could act as a platform to deliver and release the Ag^+ ions inside the bacteria cells. In the presence of a zeolite free of silver, bacteria are attached to zeolite, thus stabilized and reproduce themselves rapidly.

The behavior of both composites (z-0.1-400 and z-0.1-600) is very similar, indicating no significant effect of annealing temperature of the silver loaded zeolite on their antibacterial activity.

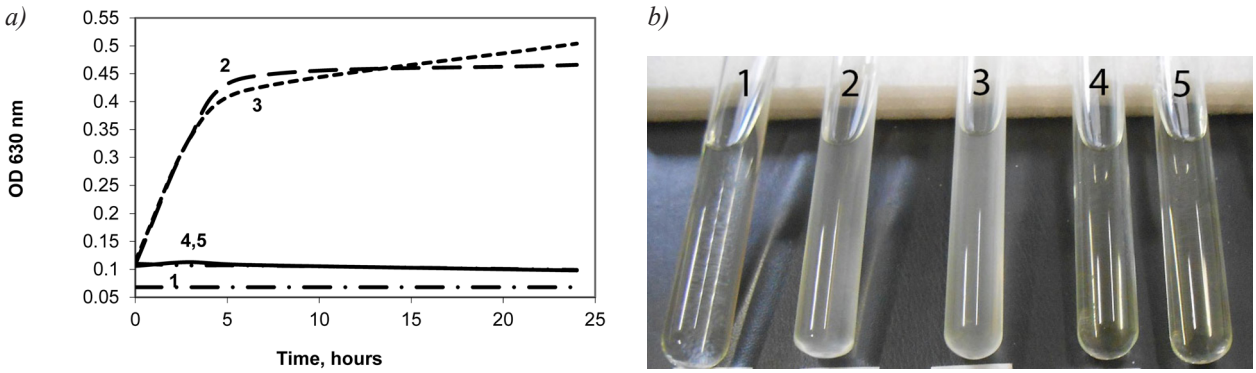

Fig. 8. Antibacterial activity of the Ag NPs-zeolite composite material – (0.1 wt%) in peptone water toward *E. coli* 3398: *1* — - — negative control; *2* — — — positive control; *3* - - - - - - sample z-0-400; *4* ——— sample z-0.1-400; *5* — - - — sample z-0.1-600.

CONCLUSIONS

As results of the study carried out the following conclusions can be drawn:

1. Zeolite loaded with Ag^+ can be used as a precursor to prepare AgNPs-zeolite composites by reduction of Ag^+ ions at elevated temperature (200–600 °C) under air conditions.

2. Composites containing around 11 wt% Ag in the zeolite have been prepared.

3. Annealing temperature of Ag-loaded zeolite does not impact the properties of AgNPs-composites.

4. The composites contain small (3–5 nm) AgNPs situated in the microstructural defects of the zeolite crystals, and bigger AgNPs (20–25 nm) that are located on the surface of zeolite crystallites.

5. The AgNPs-zeolite composites, at low amount added to Peptone water, stop the *Escherichia coli* cell growth.

Acknowledgements: *The authors thank the National Science Fund of Bulgaria for the financial support of the project DN-17/20.*

REFERENCES

1. B. L. Ouay, F. Stellacci, *Nano Today*, **10**, 339 (2015).
2. O. Eksik, A. T. Erciyes, Y. Yagci, *Pure Appl. Chem.*, **45**, 698 (2008).
3. H. Miyoshi, H. Ohno, K. Sakai, N. Okamura, H. Kourai, *J. Colloid Interface Sci.*, **345**, 2, 433 (2010).
4. T. Phothitontimongkola, K. Sanuwong, N. Siebers, N. Sukpirom, F. Unob, *Appl. Clay Sci.*, **80–81**, 346 (2013).
5. S. C. Motshekga, S. S. Ray, M. S. Onyango, M. N. B. Momba, *Appl. Clay Sci*., **114**, 330 (2015).
6. M. S.-Li Yee, P. S. Khiew, Y. F. Tan, W. S. Chiu, Y.-Y. Kok, C.-O. Leong, *Microporous Mesoporous Mater.*, **218**, 69 (2015).
7. D. Jiraroj, S. Tungasmita, D. N. Tungasmita, *Powder Technol.*, **264**, 418 (2014).
8. R. Bartolomeu, R. Bértolo, S. Casale, A. Fernandes, C. Henriques, P. da Costa, F. Ribeiro, *Microporous Mesoporous Mater.*, **169**, 137 (2013).
9. S. Meenakshi, S. Devi, K. Pandian, R. Devendiran, M. Selvaraj, *Mater. Sci. Eng.*, **C 69**, 85 (2016).
10. A. M. Hanim, N. A. N. N. Malek, Z. Ibrahim, *Appl. Surf. Sci.*, **360**, 121 (2016).
11. N. S. Flores-Lopez, J. Castro-Rosas, R. Ramirez-Bon, A. Mendoza-Cordova, E. Larios-Rodriguez, M. Flores-Acosta, *J. Mol. Struct.*, **1028**, 110 (2012).
12. L. Ferreira, A. M. Fonseca, G. Botelho, C. Almeida-Aguiar, I. C. Neves, *Microporous Mesoporous Mater.*, **160**, 126 (2012).
13. R. Guerra, E. Lima, M. Viniegra, A. Guzman, V. Lara, *Microporous Mesoporous Mater.*, **147**, 267 (2012).
14. B. Khodadadi, M. Bordbar, A. Yeganeh-Faal, M. Nasrollahzadeh, *J. Alloy Compd.*, **719**, 82 (2017).
15. K. Margeta, N. Z. Logar, M. Šiljeg, A. Farkaš, in: Water Treatment, W. Elshorbagy, R. K. Chowdhury (eds.), IntechOpen, UK, 2013, p. 81.
16. M. Panayotova, N. Mintcheva, L. Djerahov, G. Gicheva, *J. Min. Geol. Sci.*, **61**, part II, 87 (2018).
17. M. Tomašević-Čanović, *J. Serb. Chem. Soc.*, **70**, (11), 1335 (2005).
18. O. Santiago, K. Walsh, B. Kele, E. Gardner, J. Chapman, *Springerplus*, **5**, 571 (2016).
19. Y. Liu, F. Chen, S. M. Kuznicki, R. E. Wasylishen, Z. Xu, *J. Nanosci. Nanotechnol.*, **9**, 2768 (2009).
20. L. R. Harutyunyan, G. P. Pirumyan, *Proc. Yerevan State University, Chem. Biol.*, 1, 21 (2015).
21. P. Kowalczyk, M. Sprynskyy, A. P. Terzyk, M. Lebedynets, J. Namieśik, B. Buszewski, *J. Colloid Interface Sci*., **297**, 77 (2006).
22. G. V. Tsitsishvili, in: Molecular Sieves, ACS, Washington DC, 1973.
23. https://en.wikipedia.org/wiki/Ionic_radius.
24. https://en.wikipedia.org/wiki/Atomic_radii_of_the_elements_(data_page).
25. Perkin-Elmer Corporation, Handbook of X-ray photoelectron spectroscopy, Physical electronics, Minnesota, USA, 1992.
26. M. T. Anthony, M. P. Seah, *Surf. Interface Anal*., **6** (3), 95 (1984).